Transworld Research Network
37/661 (2), Fort P.O., Trivandrum-695 023, Kerala, India

Recent Res. Devel. Optics, 3(2003): 319-335 ISBN: 81-271-0028-5

18 Superresolving techniques in optical sectioning microscopy

M. T. Caballero[1], C. Ibáñez-López[2] and M. Martínez-Corral [2]
[1]Departamento de Óptica, Universidad de Alicante, PO Box 99, 03080 Alicante, Spain
[2]Departamento de Optica, Universidad de Valencia, 46100 Burjassot, Spain

Abstract

We demonstrate theoretically the feasibility of two different techniques to improve the axial resolution in optical sectioning microscopy. We propose the use of binary mask and phase only filters in conventional confocal and 4Pi-confocal systems. On the one hand, this allows one to narrow the central lobe of axial PSF, and, on the other hand, to reduce the height of the axial sidelobes which can lead to ambiguity in the image.

Introduction

The main feature of confocal scanning microscopy (CSM) is its unusually high optical sectioning capacity [1] compared with conventional three-dimensional (3D) image-formation arrangements. In spite of that, the axial resolution of such setups is still much poorer than the lateral resolution. This difference yields to an anisotropic quality of 3D images.

Correspondence/Reprint request: Dr. M. Martínez-Corral, Departamento de Optica, Universidad de Valencia, 46100 Burjassot, Spain. E-mail : Manuel.Martinez@uv.es

In this text we propose to improve the depth discrimination capacity of confocal systems by inserting spatial filters with a specified amplitude or phase transmittance at the pupil plane. Our design procedures take advantage from the multiplicative nature of the effective point-spread function (PSF) of such systems, which is given by the product between the PSF of the illumination system and the PSF of the collector one. Our PSF-engineering techniques are applied to conventional confocal microscopes and also to 4Pi-confocal microscopes, both working in the nonparaxial regime.

1. Conventional microscopy versus confocal microscopy

Let's consider a conventional 3D image-formation system, which basically consists of the telecentric arrangement shown in Fig.1. Telecentricity permits the system to be, within the frame of the first-order Born approximation, 3D linear and shift-invariant. Therefore, the 3D intensity distribution in the image space can be expressed as the 3D convolution between a scaled version of the 3D object, $O(\mathbf{r}, z)$, and the so called 3D-intensity PSF of the system, namely

$$I(\mathbf{r},z) = O(\mathbf{r},z) \otimes_3 \left|h(\mathbf{r},z)\right|^2, \tag{1}$$

where

$$h(r,z) = \int_0^1 t(\rho) \exp\left(i2\pi n \frac{\sqrt{1-\rho^2 \sin^2\alpha}}{\lambda} z\right) J_o\left(\frac{2\pi}{\lambda} nr\rho \sin\alpha\right) \frac{\sin^2\alpha}{\sqrt{1-\rho^2\sin^2\alpha}} \rho\, d\rho \,. \tag{2}$$

In this expression, $t(\rho)$ represents the amplitude transmittance of the radially-symmetric pupil, z and r denote, respectively, the axial and the radial coordinates as measured from the focus of the system, and α is the semi-aperture angle. Eq. (2) is valid in the non paraxial regime and also holds in the paraxial approximation for α small. In the later case, the exponential function becomes the defocus aberration term and then the integral corresponds to the Fourier-Bessel transform of the different defocused versions of the pupil transmittance function $t(\rho)$.

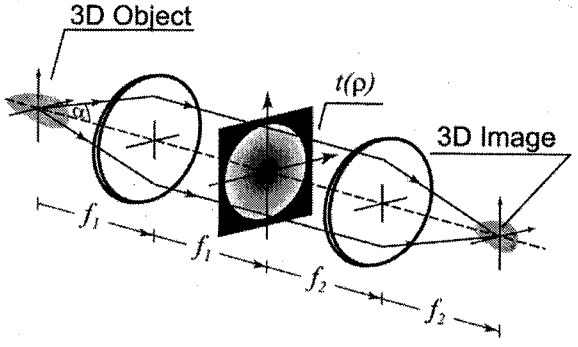

Figure 1. Schematic diagram of a conventional 3D image-formation setup.

The most important property of imaging systems when dealing with 3D object is the optical sectioning capacity, that is, the capacity of getting sharp images of the different transverse sections of the 3D object. It is also named the optical slicing capacity. In mathematical terms, the optical sectioning can be estimated by means of the so called integrated-intensity function, which evaluates the total energy of the intensity PSF at any transverse plane:

$$I_{\text{int}}(z) = \int_0^{\infty} \text{PSF}(r,z)\, r\, dr \ . \tag{3}$$

In case of a conventional system the integrated intensity is a constant. This fact is connected to the conservation of energy [2], in the sense that the total energy at every optical diffraction pattern remains constant. Consequently this kind of systems hardly have any optical sectioning capacity. Accordingly, at some plane in the image volume it appears the image of the conjugate object plane together with the blurred images of the defocused sections of the 3D object. From an ideal point of view, in order to achieve a high optical sectioning capacity the integrated intensity should be a sharp function.

A very successful alternative to conventional imaging systems is CSM. In confocal systems, the monochromatic light proceeding from a point source is focused onto a small region of the 3D object by a high numerical-aperture (NA) lens. Then, the light emitted by the sample is collected by a similar optical system and finally is detected by a point detector placed at the image plane (Fig. 2). The 3D image is built in a computer with the values of intensity acquired after 3D scanning the sample. CSM's are 3D linear and shift-invariant systems in which the 3D intensity distribution in the image can be calculated by a 3D convolution.

$$I_{conf}(\mathbf{r},z) = O(\mathbf{r},z) \otimes_3 \text{PSF}(\mathbf{r},z) \tag{4}$$

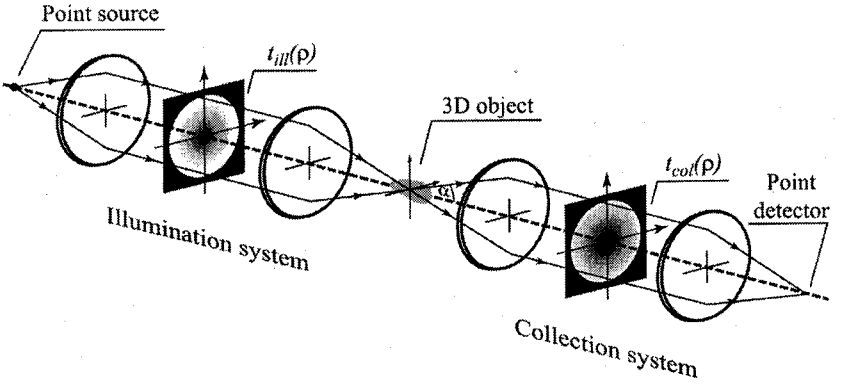

Figure 2. Schematic diagram of a confocal scanning microscope.

The intensity PSF is obtained as the product of two independent functions: the PSF of the illumination system times the PSF of the collection one:

$$\mathrm{PSF}(r,z) = |h_{ill}(r,z)|^2 |h_{col}(r,z)|^2 \tag{5}$$

In this symmetrical configuration both the illumination and the collection arms play equal roles in the imaging properties. These independent PSFs depend explicitly on the corresponding pupil function. Fig. 3 shows the 3D intensity PSF of a conventional and a confocal system. Mathematically the difference between the plots is a squared operation, which allows the confocal PSF to be sharper in both the axial and the transverse directions. However, what is more relevant, and in fact constitutes the leit motiv of confocal microscopy, is the dramatic improvement in optical sectioning capacity. This is due to the ability of confocal setups to reject the out-of-focus light. In Fig. 4 we compare the integrated intensity of a confocal system with the one corresponding to a conventional setup. We find that, since the confocal systems are non-conservative, the integrated intensity is now a sharp function.

In spite of the proverbial depth-discrimination capacity of confocal systems, they still have the drawback that, due to diffraction, the axial resolution is about three times poorer than the lateral counterpart. This difference gives rise to an anisotropic quality of the image of any 3D specimen. We propose the use of axial-apodization techniques for reducing this anisotropy.

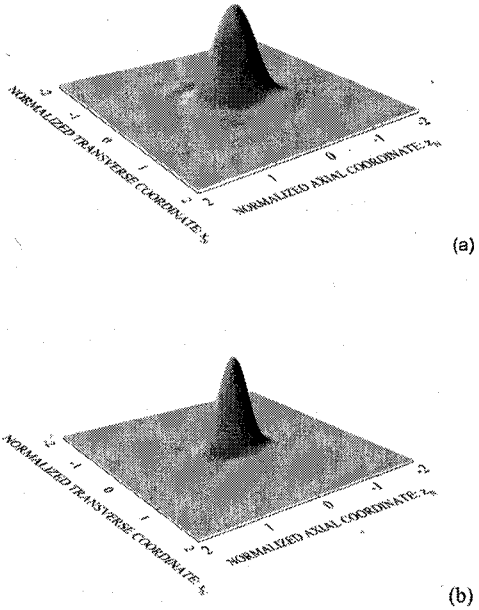

Figure 3. Meridian section of the three-dimentional intensity PSF of: (a) conventional microscope; and (b) confocal scanning microscope.

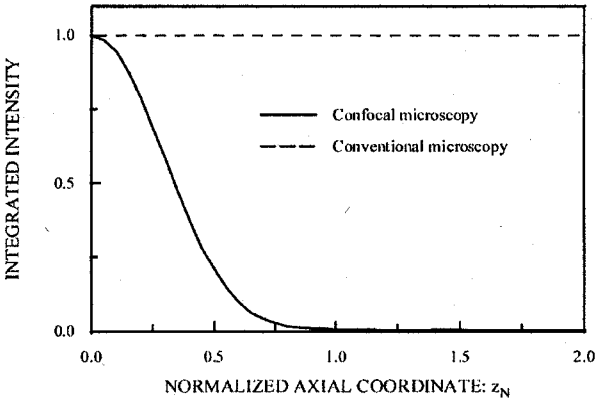

Figure 4. Integrated intensity of a conventional microscope and a confocal microscope.

2. Theory for axial apodization

Let's start our reasoning by particularizing Eq. (2) for axial points, that is

$$h(r,z) = \int_0^1 t(\rho)\exp\left(i2\pi n\frac{\sqrt{1-\rho^2\sin^2\alpha}}{\lambda}z\right)\frac{\sin^2\alpha}{\sqrt{1-\rho^2\sin^2\alpha}}\rho\,d\rho\ . \tag{6}$$

If we perform the nonlinear mapping

$$\zeta = \frac{\sqrt{1-\rho^2\sin^2\alpha}-\cos\alpha}{1-\cos\alpha}+0.5\ ;\qquad q(\zeta)=t(\rho)\ , \tag{7}$$

then Eq. (6) can be rewritten as

$$h(z_N) = \exp(i\pi z_N)\int_{-0.5}^{0.5} q(\zeta)\exp(i2\pi\, z_N\zeta)\,d\zeta\ , \tag{8}$$

where the axial position is expressed in terms of the normalized nondimensional variable

$$z_N = \frac{n}{\lambda}(1-\cos\alpha)z\ . \tag{9}$$

In the Eq. (8), the mapped function $q(\zeta)$ is zero outside the interval [-0.5, 0.5]. So, we can change the limits of the integral to plus and minus infinity. Therefore, the axial PSF is obtained from a simple 1D Fourier transformation of $q(\zeta)$.

In case of a clear circular aperture $q(\zeta)$ is a rectangle function (Fig. 5) and therefore, the 1D Fourier transform is a sine-quotient (sinc) function. Then the axial PSF of a

confocal microscope with the circular aperture inserted in both arms, is proportional to a sinc^4 function. Note that the nonlinear mapping explicitly depends on the angular aperture of the lens. Consequently a given pupil mask produces different $q(\zeta)$ profiles for different values of α. Besides, the axial extent of the focal spot is determined by the value of α through the scale factor of Eq. (9). This means that, given an optimum profile for $q(\zeta)$, the actual pupil transmittance must be calculated explicitly for the NA value of interest.

Note that the Eq. (9) is wavelength dependent. In case of confocal microscopes working with fluorescence samples, the wavelengths for illumination and collection are different. Consequently the corresponding PSFs have different scales (see Fig. 6), so that the confocal PSF is now given by:

$$\text{PSF}(r, z_N) = \left|h_{ill}(r, z_N)\right|^2 \left|h_{col}(\varepsilon r, \varepsilon z_N)\right|^2 \tag{10}$$

where $\varepsilon = \lambda_{ill}/\lambda_{col}$.

Since we are interested in the design of filters for narrowing the axial PSF, it is convenient to develop the concept of axial gain in resolution. To this end it is necessary

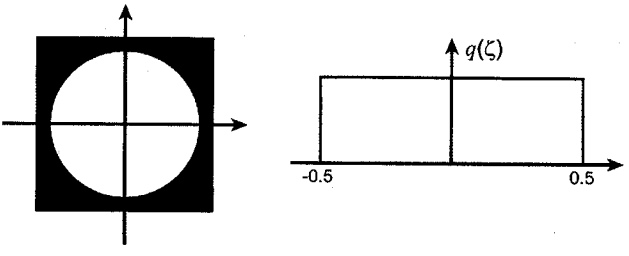

Figure 5. Mapped function of a clear circular aperture.

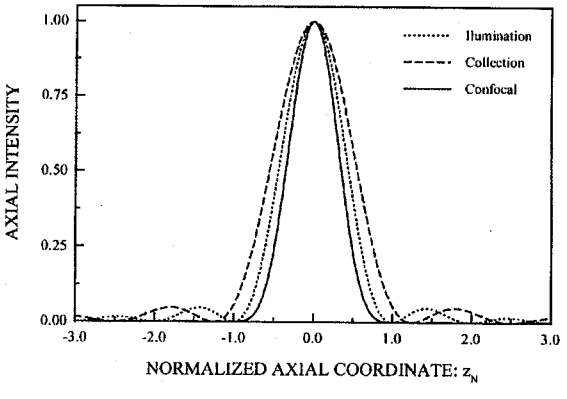

Figure 6. Axial intensity PSFs of a confocal fluorescence scanning microscope. In the calculations we considered $\varepsilon = 0.8$.

to expand the normalized intensity into Taylor series within second-order approximation [3, 4], that is

$$I_N(0, z_N) = \frac{|h(0, z_N)|^2}{|h(0,0)|^2} \approx 1 - 4\pi^2 \left(\frac{z_N}{1/\sigma} \right)^2 \tag{11}$$

where σ represents the standard deviation of $q(\zeta)$, namely:

$$\sigma = \sqrt{\frac{m_2}{m_0} - \frac{m_1^2}{m_0^2}}, \quad m_n = \int_{-0.5}^{0.5} q(\zeta) \zeta^n \, \mathrm{d}\zeta \quad . \tag{12}$$

Then we define the axial resolution gain as

$$G_A = \frac{\sigma}{\sigma_c} \tag{13}$$

where subscript c corresponds to the nonapodized circular pupil. The conclusion is clear to obtain axial resolution σ must be greater than σ_c.

3. Apodization in conventional confocal microscopy

On the basis of the above ideas, we propose different axially superresolving filters. The choice of binary filters yields a design that can be manufactured with relative ease. Then $q(\zeta)$ should be binary and with a standard deviation higher than the corresponding to the circular aperture. To fulfil these constraints we designed a set of filters whose mapped transmittance consists in two equal-width rectangles. The smaller the width, the higher the axial gain in resolution. This design gave rise to the so-called dark-ring (DR) filters, which are composed by two concentric transparent rings. The area of the rings depends on the angular aperture of the lens (Fig. 7) In the paraxial regime two equal-width rectangles in the mapped space become two equal-area rings. In case of high angular aperture, the rings have no longer the same area. This is because the contribution to the focal field from the outer parts of the pupil wave-front is higher than the contribution from the inner parts.

If we insert a DR filter in the illumination-path pupil of a confocal system, and a circular aperture in the collection-path pupil, we obtain a 3D confocal PSF that has been importantly narrowed in the axial direction. Besides the PSF remains almost constant in the transverse direction. In Fig. 8 we can see that some small sidelobes appear due to the use of the proposed filters. However, the sidelobes are so small that they do not compromise the effective gain in resolution. So, we have shown that by simply inserting a binary filter in the illumination arm of a confocal setup, the anisotropy of the PSF can be importantly reduced.

When confocal scanning systems are used for imaging fluorescent samples, the light efficiency of the imaging system is a matter of special interest. Because of that, in the case of fluorescent images, it is more convenient the design of phase-only pupil filters. To obtain a desired axial distribution it is necessary to solve an inverse problem and

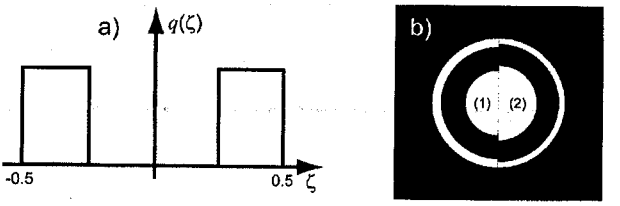

Figure 7. The dark-ring binary filter: (a) mapped transmittance; (b) actual 2D representation for the cases of $\alpha = 10°$ (1) and $\alpha = 67.5°$ (2). Note that the form of the pupil strongly depends on the value of α.

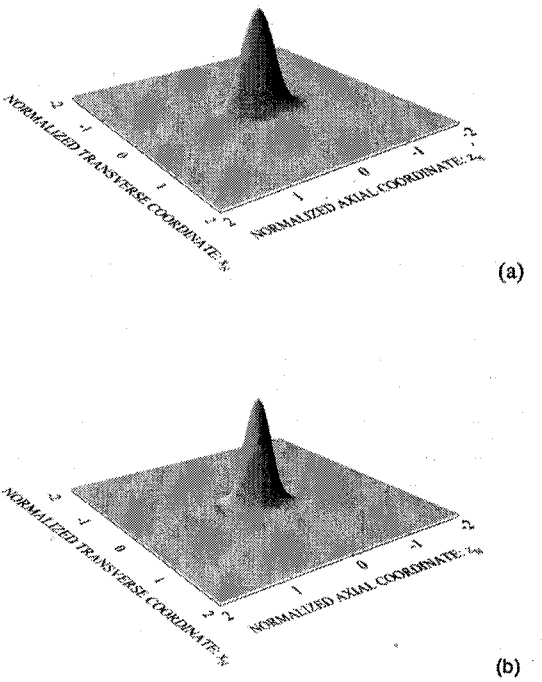

Figure 8. (a) 3D intensity PSF of a confocal microscope with two circular pupils; (b) same as (a) but with the dark-ring filter in the illumination system.

design a mapped function $q(\zeta)$, which is in general a non-trivial task. An alternative approach is based on the Toraldo concept [5]. Toraldo di Francia showed that the radii of the zero-intensity rings in the focal plane of a paraxial focusing system can be selected at will by using a pupil filter subdivided into concentric zones with constant transmittance. In the original Toraldo algorithm the amplitude transmittance of the filter, $t(\rho)$, is subdivided into m concentric annular zones to control the radii of m-1 rings of zero intensity.

We show that by applying the Toraldo concept to the mapped version of the pupil transmittance, it is possible to control the positions of a finite number of zeros of the axial PSF. Moreover, since the axial PSF is a matter of interest in 3D imaging systems in which the lenses have high numerical aperture, such as confocal microscopy, we have extended the Toraldo method to the case of nonparaxially focused fields. In our approach the function $q(\zeta)$ is also subdivided into constant-transmittance zones. Here it is important to take into account that if one wants to tailor the axial PSF with the constraint that the transverse PSF should remain almost invariant, the resulting function $q(\zeta)$ must be an even function. This implies that to control the positions of m-1 axial zeros, the interval [-0.5, 0.5] should be divided into $2m$-1 subintervals where the function $q(\zeta)$ is constant.

The procedure for shaping the axial intensity of nonparaxially focused scalar fields is as follows [6]. First, the function $q(\zeta)$ is decomposed as:

$$q(\zeta) = k_1 \mathrm{rect}\left(\frac{\zeta}{\Delta_1}\right) + \sum_{i=1}^{m-1} k_{i+1}\left[\mathrm{rect}\left(\frac{\zeta}{\Delta_{i+1}}\right) - \mathrm{rect}\left(\frac{\zeta}{\Delta_i}\right)\right], \tag{14}$$

where $\Delta_m = 1$, $\Delta_i > \Delta_{i-1}$, $m \geq 2$, and k_i is the transmittance of the i^{th} zone.

According to Eq. (8) the axial amplitude PSF of this filter is given, apart from irrelevant constant factors, by the 1D Fourier transform of $q(\zeta)$, that is:

$$h(0, z_N) = \sum_{i=1}^{m} k_i \left[\Delta_i \ \mathrm{sinc}(\Delta_i \, z_N) . - \Delta_{i-1} \ \mathrm{sinc}(\Delta_{i-1} \, z_N)\right] . \tag{15}$$

In the simplest case, corresponding to $m = 2$ (Fig. 9), which allows one to control the position of one zero, the axial amplitude PSF is given by:

$$h(0, z_N) = (k_1 - k_2)\Delta \mathrm{sinc}(\Delta z_N) + k_2 \mathrm{sinc}(\Delta z_N) \tag{16}$$

where $\Delta = \Delta_1$.

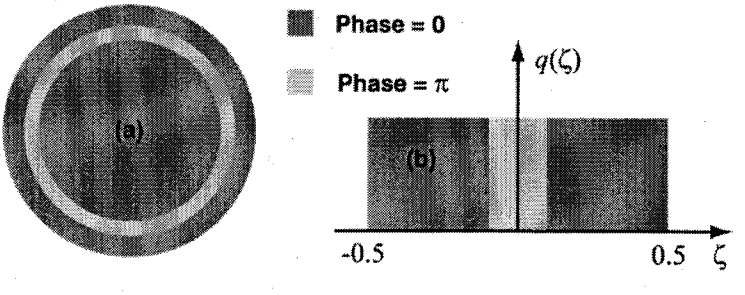

Figure 9. Three-zone Toraldo filter; (a) 2D representation for the case $\alpha = 67.5°$; (b) mapped transmittance.

If we apply now the design constraint, that is, we force the axial amplitude to be zero at a selected point, say $z_N = z_1$:

$$(k_1 - k_2)\Delta\mathrm{sinc}(\Delta z_1) + k_2\mathrm{sinc}(\Delta z_1) = 0 \ , \tag{17}$$

and we maximize the filter throughput, making that the two zones have no absorption and opposite phases:

$$k_2 = -k_1 = 1 \tag{18}$$

we obtain the transcendental equation

$$\Delta = \frac{\mathrm{sinc}(z_1)}{2\mathrm{sinc}(\Delta z_1)} \tag{19}$$

whose root is the abscissa of point of intersection of the curve $y = \mathrm{sinc}(z_1)/\mathrm{sinc}(\Delta z_1)$ and the straight line $y = 2\Delta$.

To establish the usefulness of the method we consider the case of an axially superresolving pupil filter, that is, a filter that shapes the axial PSF such that the extent of the central lobe is narrowed by an arbitrary factor, which we set to 0.7 in the present example. Since in the case of the circular pupil, for which $q(\zeta) = \mathrm{rect}(\zeta)$, the first axial zero appears at $z_N = 0.7$, then the value of the constraint parameter should be $z_1 = 0.7$. The solution of the transcendental Eq. (19) is then $\Delta = 0.19$. In Fig. 10 we compare the normalized axial intensity PSF provided by the Toraldo filter with that corresponding to the nonapodized circular pupil. Note that the use of the Toraldo filter gives rise to an axial distribution in which the narrowness of the central lobe is accompanied by the enlargement of outer lobes.

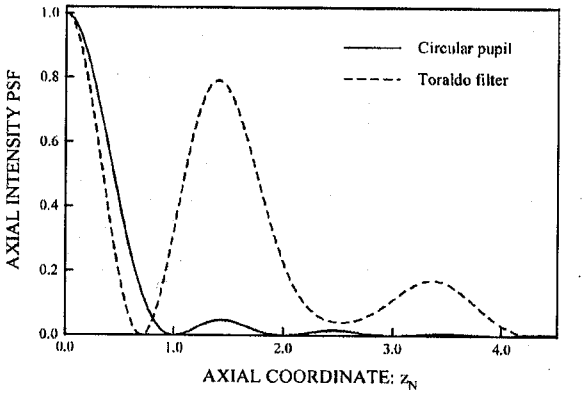

Figure 10. Normalized axial intensity PSF corresponding to the circular pupil and to the three zone Toraldo filter.

What we propose here is to place the Toraldo filter in the illumination and a circular aperture in the collection (to avoid light losses in the collection process). In this case, the resulting confocal-system PSF is narrowed in the axial direction, compared to the corresponding to the nonapodized confocal system, and the high axial sidelobes disappear. In the Fig. 11 we show the illumination PSF and the confocal PSF in one of those systems.

Note that we should consider not only the form of the confocal PSF, but also the form of the illumination PSF. This is because the presence of high sidelobes in the illumination PSF could result in significant photobleaching of the 3D specimen at the positions of the strong secondary peaks. This fact yields artifacts in the images that must be avoided. This problem is overcome by designing filters with a high number of zones. Specifically we found that with the seven-zone Toraldo filter one can control the effect of photo-bleaching by sending the huge axial sidelobe far away (Fig. 12). Note that in this case, the design procedure is adapted to the size of the fluorescent sample, to ensure that the axial sidelobes remain outside the sample during imaging. In this example, samples up to $z_N = 4$ thick can be imaged without bleaching by the sidelobes. The use of the Toraldo filter narrows the intensity PSF, along the optical axis, and therefore provides an important improvement of the optical sectioning capacity (Fig. 13)

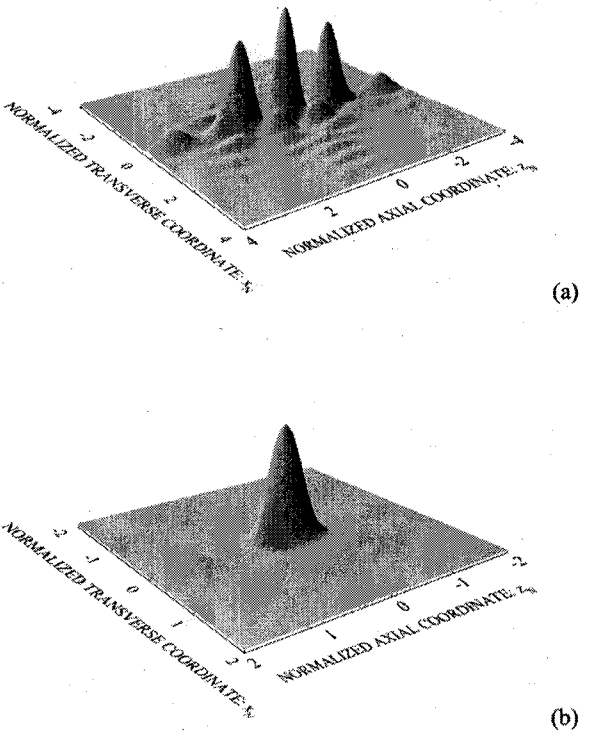

Figure 11. (a) 3D illumination intensity PSF corresponding to the three-zone Toraldo filter; (b) 3D intensity PSF of a confocal system whose illumination pupil is apodized with the Toraldo filter.

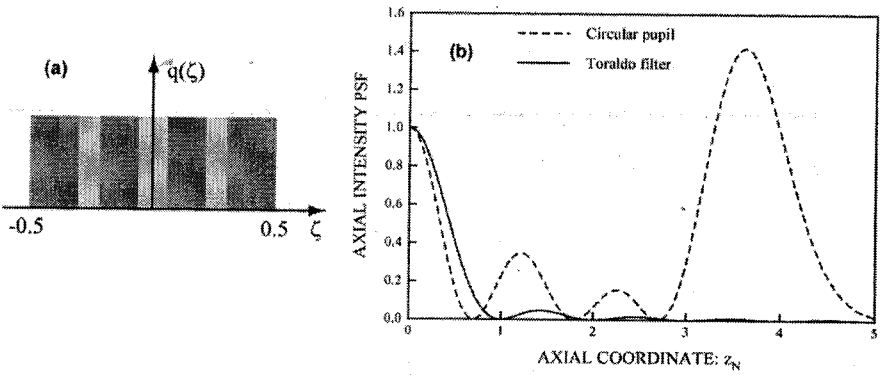

Figure 12. a) Seven zone Toraldo filter designed for obtaining axial superresolution in confocal fluorescence microscopy. b) the corresponding axial intensity PSF

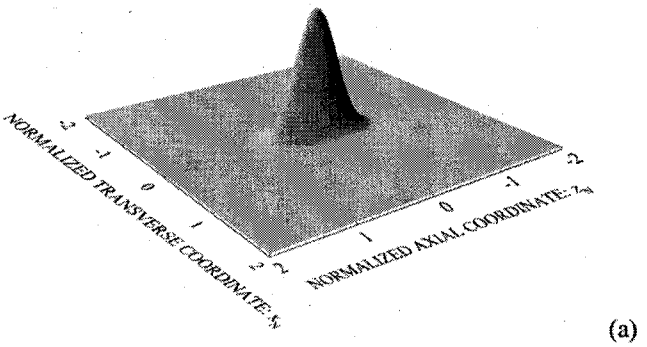

(a)

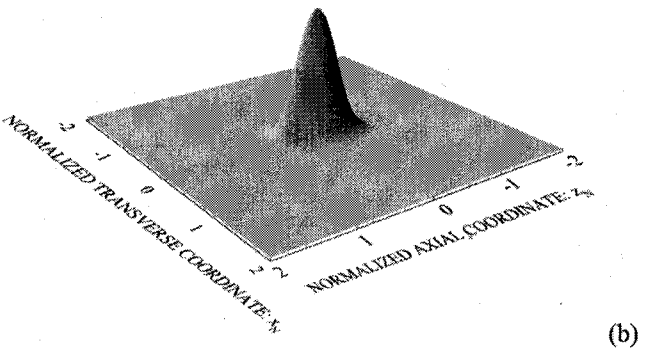

(b)

Figure 13. a) 3D intensity PSF of a confocal microscope with two circular pupils; b) same as (a) but with the seven-zone Toraldo filter in the illumination system.

4. Apodization in 4Pi-confocal microscope

A very ingenious, and efficient, technique for reducing the axial extent of the PSF is to create a standing wave by the interference of two opposing wave-fronts, as made in 4Pi microscopy [7]. In this system, two opposing high-NA objectives are used for illuminating coherently and detecting the same point of a fluorescent specimen (Fig. 14). According to Eq. (10), the 3D PSF of this imaging system is given by:

$$\mathrm{PSF}(r,z_N)=\left|h_{ill}(r,z_N)+h_{ill}(r,-z_N)\right|^{2m}\cdot\left|h_{col}(\varepsilon r,\varepsilon z_N)+h_{col}(\varepsilon r,-\varepsilon z_N)\right|^2 \tag{20}$$

where the parameter m defines the mode of excitation, e.g. m=l denotes single-photon absorption.

The resulting PSF has an axial main peak that is about four times narrower than its confocal counterpart (Fig. 15). However, the narrowing of the main peak is accompanied by a severe enlargement of the secondary axial sidelobes, which causes ambiguity in the image. To avoid the sidelobes problem, it was classically proposed the use of two-photon absortion (m = 2) [8]. In such case, the contribution of the secondary maxima of the illumination PSF is importantly reduced due to the squared dependence of the excitation on the illumination intensity.

An alternative technique for reduction of axial sidelobes consists of placing a pair of properly-designed annular filters in the illumination path of a single-photon 4Pi(C) confocal microscope [9]. As in conventional confocal microscope, we insert the filters in the illumination path to avoid waste of fluorescence light. The idea is to allow the secondary peak of the illumination PSF be multiplied by low values of the detection PSF and the secondary peaks of the detection PSF be multiplied by low values of the illumination PSF. The multiplicative process will yields to a significant reduction of the axial sidelobes of the 4Pi-system PSF

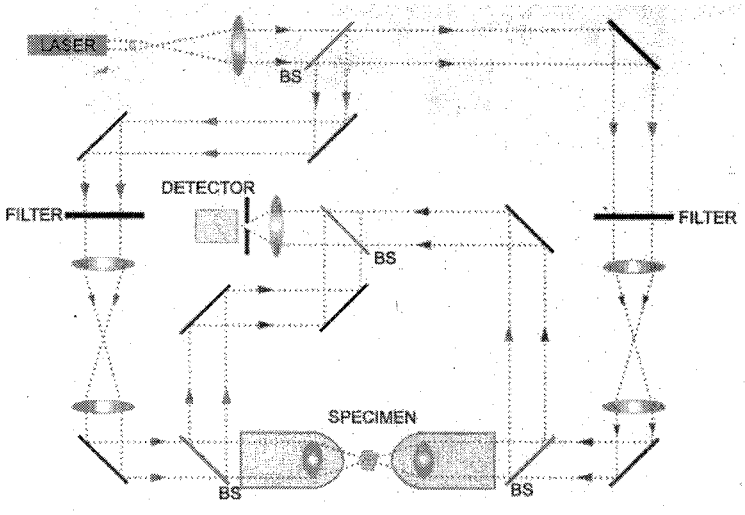

Figure 14. Schematic set-up of a 4Pi(C) confocal microscope

In the process of design it is necessary to take into account that the PSF-sidelobe-reduction capacity of the filters depends on the width of the rectangles, (Fig. 7), and, in accordance with Eq. (10) the sidelobe height depends strongly on the value of ε. In Fig. 16 we have depicted the axial PSF of a 4Pi(C)-confocal microscope that incorporates the selected filter in the illumination set. Note, by comparing the curves in the figure, that the use of the binary mask produces a severe reduction in the sidelobe strength. Specifically, the relative height of the side-lobe is ~5% of the main peak.

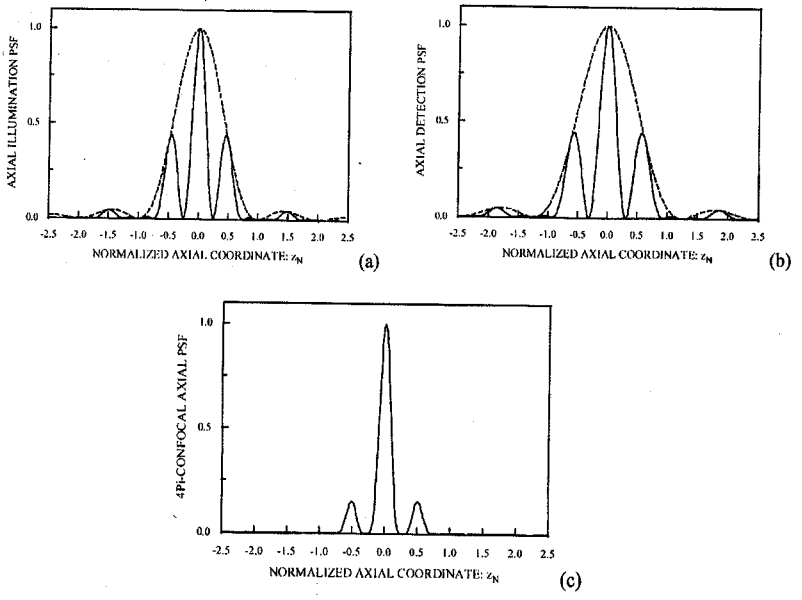

Figure 15. a) axial intensity PSF of the illumination arm of a 4Pi-confocal microscope; b) same but for the detection arm (dashed curves correspond to the enveloping function); c) intensity PSF of a 4Pi(C)- confocal microscope.

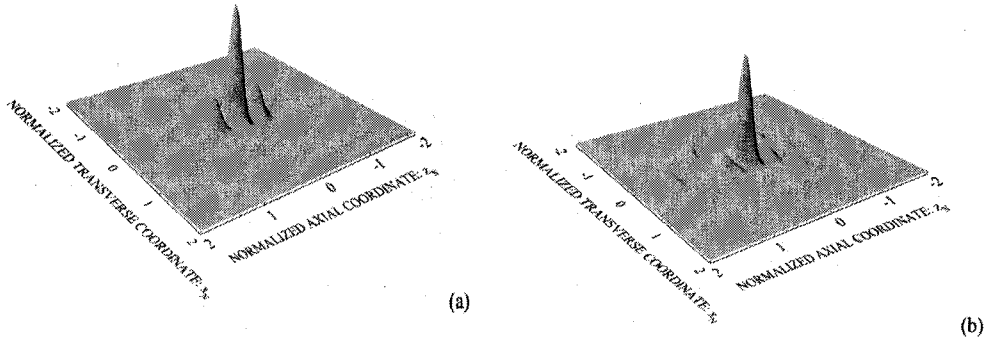

Figure 16. Numerically evaluated axial intensity PSF of a 4Pi(C)-confocal microscope with: a) the circular pupil in the illumination set; b) the binary filter in the illumination set.

Also, we centre our attention on analyzing the form of the axial PSF of the illumination part of the 4Pi(C) microscope. As it is shown in Fig. 17 the use of the proposed annular filter reduces the first axial-sidelobe strength but it produces a severe enlargement of other secondary peaks. This effect can be overcome by using an annular filter but with higher efficiency, at the expense of a lower reduction of the sidelobe height of the combined system PSF.

Another alternative technique is the use of Toraldo filters [10]. Since the zones have no absorption, with this method, it is possible to avoid losses of light in the illumination process and to optimize the throughput of the filter. To show the power of this proposal, we use a seven zone Toraldo filter in single photon 4Pi(C) system. The effect is similar to the one produced by two-photon absorption, that is, the sidelobes are downed to 7% of the main peak, which is 3.3 times lower than the lobe height obtained without the Toraldo filter. (Table 1). Also, we compare, in Fig. 18, the 3D intensity corresponding to the single-photon 4Pi(C) confocal microscope with and without the seven zone Toraldo filter. Note that apart form strongly reducing the axial sidelobes, the use of Toraldo filters hardly affects to the transverse resolution.

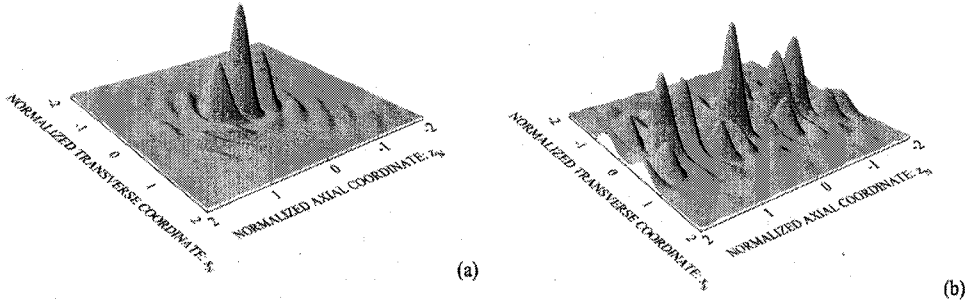

Figure 17. 3D intensity PSF of the illumination part of a 4Pi(C)-confocal microscope. a) with-out apodization and b) with the seven-zone Toraldo mask.

Table 1. List of PSF figures of a single-photon 4Pi (C), a two-photon 4Pi (C) and a single-photon 4Pi (C) with Toraldo filters.

	Axial intensity PSF	
	FWHM	Sidelobe relative height
4Pi(C), m=1	63 nm (100%)	0.23 (100%)
4Pi(C), m=2	76 nm (121%)	0.03 (13%)
4Pi(C), m=1 with Toraldo filters	61 nm (97%)	0.07 (30%)

Finally, we demonstrate the viability of Toraldo filters in 4Pi-confocal microscopy with anumerical simulation (Fig. 19). Since confocal systems are linear and shift invariant systems, it is possible to obtain the image with a convolution between the object and the PSF of the system. Note that the image with apodized 4Pi(C)-confocal microscope is better, in axial direction, than one with nonapodized 4Pi(C)-confocal microscope. Furthermore, in transverse direction, the differences are not appreciable.

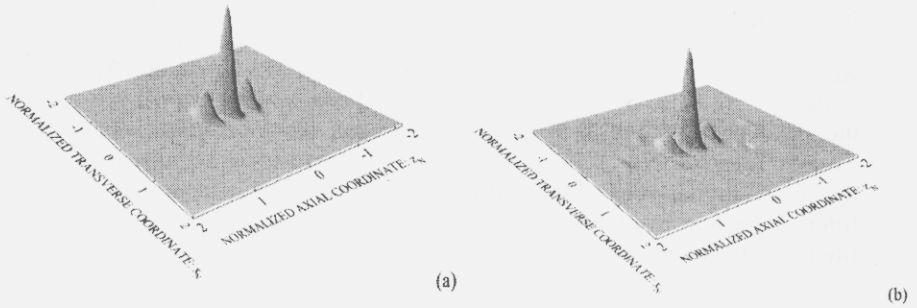

Figure 18. Contour plot of the 3D intensity PSF corresponding to: a) 4Pi(c) single-photon confocal microscope; and b) same as (a) but with the seven-zone Toraldo filters inserted in the illumination path

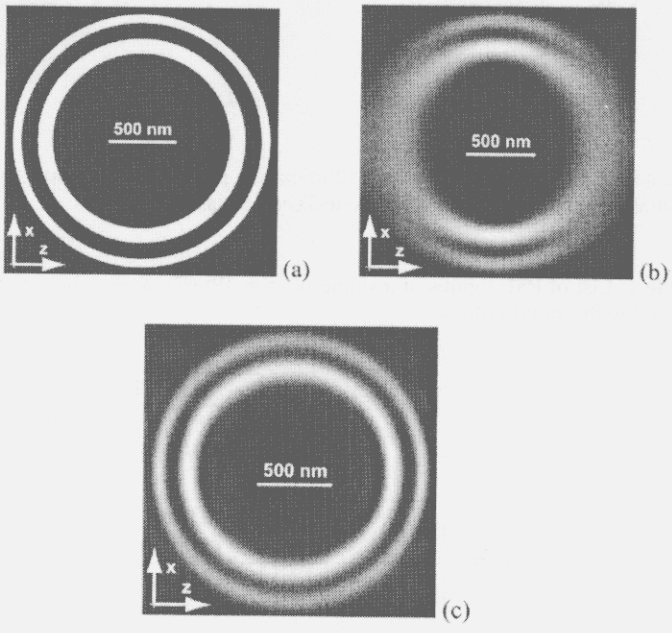

Figure 19. Numerical experiment: a) Object, b) image through 4Pi(C) confocal microscope and c) image through 4Pi(C) confocal microscope with Toraldo filters.

5. Conclusions

We have designed two different techniques for apodization in confocal scanning microscopes in which the objectives have high-NA. With both of them, binary and only-phase Toraldo filters, we obtain axial superresolution and a decrease of sidelobes height of 3D intensity. Nevertheless, in fluorescence applications, it is necessary to take into account that the presence of high sidelobes in the illumination PSF could result in significant photo-bleaching of the 3D specimen. The use of Toraldo filters lets control the axial zero positions and therefore, the design can be adapted to the thickness of the sample to ensure that the axial sidelobes remain outside the sample during imaging.

6. Acknowledgements

This work was funded by the Plan Nacional I+D+I (Grant DPI2000-0774), Ministerio de Ciencia y Tecnología, Spain. C. Ibáñez-López gratefully acknowledges financial support from the same institution.

7. References

1. T. Wilson, *Confocal Microscopy*, Academic, London (1990).
2. J. W. Goodman, *Introduction to Fourier Optics*. McGraw-Hill, New York, 2nd Ed. (1996)
3. M. Martínez-Corral, P. Andrés, J. Ojeda-Castañeda and G. Saavedra, *Tunable axial superresoltion by annular binary filters. Application to confocal microscopy*. Opt. Commun. **119**, 491-498 (1995)
4. C. J. R. Sheppard and Z. S. Hegedus, *Axial behaviour of pupil-plane filters*. J. Opt. Soc. Am. A **5**, 643-647 (1988)
5. G. Toraldo di Francia, *Nuovo pupille superresolventi*. Atti Fond. Giorgio Ronchi **7**, 366-372 (1952)
6. M. Martínez-Corral, M. T. Caballero, E. H. K. Stelzer and J. Swoger, *Tailoring the axial shape of the point spread function using the Toraldo concept*. Opt. Express, **10**, 98-103 (2002)
7. S. Hell and E. H. K. Stelzer. *Properties of a 4Pi confocal fluorescence microscope*. J. Opt. Soc. Am. A **9**, 2159-2165 (1992)
8. S. Hell and E. H. K. Stelzer, *Fundamental improvement of resolution with a 4Pi-confocal fluorescence microscope using two-photon excitation*, Opt. Commun., **93**, 277-282 (1992)
9. M. Martínez-Corral, M. T. Caballero and A. Pons, *Axial apodization in 4Pi-confocal microscopy by annular binary filters*, J. Opt. Soc. Am A, **19**, 1532-1536 (2002).
10. M. Martínez-Corral, M. T. Caballero and A. Pons, *Sidelobe decline in single-photon 4Pi microscopy by Toraldo rings*. Micron (in press).